Journal of Alloys and Compounds 919 (2022) 165806

Contents lists available at ScienceDirect

Journal of Alloys and Compounds

journal homepage: www.elsevier.com/locate/jalcom

Internal friction associated with ε martensite in shape memory steels produced by casting route and through additive manufacturing: Influence of thermal cycling on the martensitic transformation

L. Del-Río[a], M.L. Nó[a], A. Sota[b,c], I. Perez-Casero[b], J.F. Gómez-Cortés[a], M. Pérez-Cerrato[a], A. Veiga[b,c], I. Ruiz-Larrea[a], S. Ausejo[b,c], N. Burgos[b,c], J.M. San Juan[a,*]

[a] Dpt. Física, Facultad de Ciencia y Tecnología, Universidad del País Vasco, UPV/EHU, Apdo 644, 48080 Bilbao, Spain
[b] CEIT-Basque Research and Technology Alliance, BRTA, Manuel de Lardizabal 15, 20018 Donostia/San Sebastian, Spain
[c] Universidad de Navarra, Tecnun, Manuel de Lardizabal 13, 20018 Donostia/San Sebastian, Spain

ARTICLE INFO

Article history:
Received 28 April 2022
Received in revised form 26 May 2022
Accepted 6 June 2022
Available online 8 June 2022

Keywords:
Shape memory alloys
Fe-Mn-Si-Cr-Ni
Martensitic transformation
Internal friction
Additive manufacturing

ABSTRACT

Among the different families of shape memory alloys (SMA), the Fe-Mn-Si-Cr-Ni alloys have attracted a renewed interest because of its low cost, high corrosion resistance and high recovery strength during the shape memory effect, and the new technologies of additive manufacturing offer unforeseen possibilities for this family of SMA. In the present work, the reversible γ − ε martensitic transformation (MT), responsible for the shape memory effect, is studied in two Fe-Mn-Si-Cr-Ni alloys with high (20.2 wt%) and low (15.8 wt%) Mn content, produced by the conventional route of casting and rolling, in comparison with the MT in another similar alloy, with intermediate Mn content (19.4 wt%), which was produced by gas atomization and additive manufacturing through laser metal deposition. The forward and reverse γ − ε MT is studied by mechanical spectroscopy through the internal friction spectra and the dynamic modulus variation, together with a parallel microstructural characterization including in-situ observation of the γ − ε MT during cooling and heating at the scanning electron microscope. The evolution of the transformed fraction of ε martensite, evaluated through the integral area of the internal friction peak, was followed along thermal cycling in all three alloys. Both, the internal friction and the electron microscopy studies show that the ε martensite amount increases very fast during the first few cycles, and then decreases with a tendency towards its stabilization for many tens of cycles. The results show that the γ − ε MT is more stable on cycling in the additive manufactured sample than in the conventionally processed samples, opening new avenues for designing shape memory steels to be specifically processed through additive manufacturing.

1. Introduction

Among the different ferrous shape memory alloys (SMA), the family of Fe-Mn-Si-based alloys is attracting a renewed interest in the last decade, because of its low cost, good corrosion resistance and high strength during shape memory behavior. The Fe-Mn-Si SMA was first discovery by Sato et al. [1,2] in single crystals and then by Murakami et al. [3] in polycrystals, being further developed the Fe-Mn-Si-Cr-Ni as a new kind of stainless steels, whose shape memory behavior is associated with the martensitic transformation from the cubic austenite γ (FCC) to the hexagonal martensite ε (HCP), see references [4–6] for an overview on the earlier works in this field. The nucleation and growing of the ε martensite can be reversible, being responsible for the shape memory effect, whereas the concurrent α' (BCC) martensite does not give any shape memory effect and can even prevent the reversible behavior of ε when both martensite coexist [1].

In contrast with the currently used Ti-Ni [7,8] or Cu-Al-based [9,10] SMA, the Fe-Mn-Si SMA are non-thermoelastic and do not exhibit superelastic effect, but only shape memory effect [5,6]. However, the high strength during recovery in shape memory effect allows these SMA to found number applications in coupling systems [11–13], as well as self-healing composites [14–16] and seismic damping [17–19] in civil engineering associated with ε martensite. In the last decade, the design of these SMA converges with the high-Mn TRIP (Transformed Induced Plasticity) steels, being named shape memory steels [20,21], opening new applications in several industrial sectors. At present the effort is focused on the

* Corresponding author.
E-mail address: jose.sanjuan@ehu.es (J.M. San Juan).

https://doi.org/10.1016/j.jallcom.2022.165806
0925-8388/

Table 1
Composition (wt%), processing method and thermal treatments of post-processing, for the three studied alloys.

	Composition (wt%)					Processing method	Thermal treatment
	Fe	Mn	Si	Cr	Ni		
FMS3	Balance	20.2	5.2	8.5	5.0	Cast and rolling	Annealing at 1200 K + ice-water quenched
FMS4	Balance	15.8	6.1	9.2	5.0	Cast and rolling	Annealing at 1350 K + ice-water quenched
LMD	Balance	19.4	5.9	9.2	5.1	Additive manufacturing LMD	Annealing at 1350 K + ice-water quenched

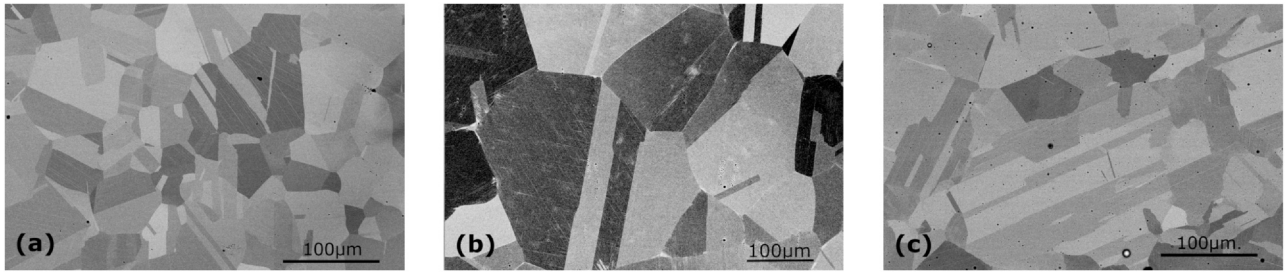

Fig. 1. Scanning electron microscopy BSE images for (a) FMS3, (b) FMS4, (c) LMD samples after recrystallization thermal treatment and ice-water quenching.

microstructural design and the key processing parameters to obtain a large recoverable shape memory strain [21,22]. In parallel, the new paradigm of the materials processing by additive manufacturing (AM) [23,24] is also being applied to SMA and in particular to the Ti-Ni-based families of SMA [25]. Nevertheless, there is a lack of information concerning the possibility and capabilities of Fe-Mn-Si-based SMA processed by AM. Then, the present study was approached on Fe-Mn-Si-Cr-Ni SMA because they exhibit a high corrosion resistance, and are expected to be better adapted for additive manufacturing.

Then, the aim of the present work is to analyze the $\gamma - \varepsilon$ martensitic transformation in a comparative study between the Fe-Mn-Si-Cr-Ni SMA produced by the conventional route of casting and hot rolling, and the ones produced by gas atomization and additive manufacturing by laser metal deposition (LMD). The characterization of the reversible $\gamma - \varepsilon$ martensitic transformation is approached by mechanical spectroscopy [26], because it is a powerful tool for analyzing structural phase transitions, which in parallel is complemented with the microstructure characterization through electron microscopy. The goal of the present work is to compare the cycling behavior of the $\gamma - \varepsilon$ martensitic transformation in both kind of differently processed SMA.

2. Materials and methods

2.1. Samples and processing methods

Three different alloys were studied within the family of Fe-Mn-Si-Cr-Ni SMA. On the one hand, ingots of two alloys with high and low Mn content, Fe-20.2Mn-5.2Si-8.5Cr-5Ni (FMS3) and Fe-15.8Mn-6.1Si-9.2Cr-5Ni (FMS4) were elaborated by the usual processing route of melting and casting and subsequently hot rolling into plates of 0.5 mm thickness [27]. The compositions of the alloys were measured by ICP (Inductively Coupled Plasma), and are presented in Table 1. On the other hand, a third alloy was designed with an intermediate Mn and Si content with respect of the previous ones, in order to maintain the temperatures of the martensitic transformation and decrease the Neel temperature T_N according to the previous works on the influence of Mn and Si on T_N [3,28], which indicate that Mn increases T_N whereas Si decreases T_N. Indeed, at T_N the austenite γ undergoes a magnetic transition from a paramagnetic state at high temperature to an anti-ferromagnetic state when cooling below T_N, which decreases its energy and hinders the martensitic transformation [27,29,30]. In addition, in Fe-Mn-Si alloys Mn contents lower than 20% are prone to produce α' martensite with negative effect on the shape memory effect. With these criteria, we selected only one composition to develop the prototype alloy for the production through additive manufacturing. Powders of the alloy were produced by gas atomization at the CEIT technology center being sieved and analyzed by ICP, with a final composition of Fe-19.4-Mn-5.9Si-9.2Cr-5.1Ni, see Table 1. The powders were processed by Laser Metal Deposition (LMD) technology using a KukaKR30 with an ytterbium source with the following processing parameters: laser power of 1150 W, scanning velocity of 665.7 mm/min, powder flux of 9 g/min and a spot of 2 mm.

Further thermal treatments were carried out above the recrystallization temperature of each alloy, 1200 K for FMS3 [31] and 1350 K for FMS4 and LMD samples, intending to obtain an austenitic phase γ containing a rather low density of dislocations [27]. All samples were annealed in an argon atmosphere and ice-water quenched. The corresponding thermal treatments and chemical composition of each alloy are listed in Table 1. Fig. 1 shows the microstructure of each sample after the thermal treatment; the three alloys contain a predominance of γ (austenite) phase and traces of ε (martensite) phase, probably induced by the increasing stresses during quenching. The grain size is about 100–150 µm for FMS4 and LMD samples and slightly smaller for FMS3 sample, as expected from the lower temperature of the recrystallization annealing.For the study of the MT evolution on cycling, the samples were initially cycled inside the torsion pendulum for the first ten cycles. However, for studying the influence of higher number of cycles, the samples were dismounted and cycled away by immersing the specimen in liquid nitrogen (for the forward MT) and in a sand heating plate Selecta LHG at 500 K. Then, the samples were mounted again in the torsion pendulum for further IF measurements. This procedure is justified because the applied stress involved in mechanical spectroscopy is very low, even to produce the stress induced martensitic transformation, and during measurements this stress act as a probe to detect the motion of the martensite interfaces, which in fact are thermally induced during cooling. So it is not expected any influence of the applied stress used during IF measurements on the cycling behaviour. Indeed, previous works in a similar alloy [27,29] showed that the cycles performed inside and outside the pendulum follows the same trend on cycling behavior.

2.2. Mechanical spectroscopy and electron microscopy

Mechanical spectroscopy experiments were carried out in a subresonant inverted torsion pendulum working under a low-pressure Helium atmosphere of 4 mbar, in a frequency range from 10^{-3} to 5 Hz, and at different heating-cooling rates in a temperature range between 100 K and 1150 K [32]. Samples of approximately $40 \times 5 \times 0.8\ mm^3$ were cut for the internal friction (IF) and dynamic modulus (DM) measurements, and for the present research a constant strain amplitude of $\varepsilon_0 = 2 \times 10^{-5}$, established in austenite phase at room temperature, was used for all measurements. To design the experiments, the dependences of the internal friction peak strength on the heating-cooling rate and on frequency [33] were considered, and a constant heating-cooling rate of 1.5 K/min and a frequency of 0.5 Hz were selected to work in the whole temperature range, which was chosen so that the whole interval Mf-Af was completed, from 100 K to 510 K. However, due to the cooling system of the pendulum, the cooling rate can not be kept when approaching 100 K, resulting in the lessening of the IF peak of the direct transformation, since the peak strength is proportional to the cooling rate. Nevertheless, in a previous work in this kind of alloys [29] it was demonstrated that the integral of the IF peak during the forward transformation on cooling is equal to the one during the reverse transformation on heating. Consequently, in the present work the transformed fraction corresponding calculus was made utilizing the data of the reverse transformation.

The microstructural characterization was conducted via electron microscopy techniques. The specimens were prepared by conventional mechanical polishing (Struers Abramin), followed by electropolishing (Struers ElectroPol-5) with a solution of 700 ml of ethanol, 100 ml of glycerin and 200 ml of HClO4, at 10–12 V and room temperature, up to 180 s. This final electropolishing step was very useful to have a better definition in backscatter electron images (BSE mode) and to remove the stress-induced martensites artificially introduced at the surface of the sample during the mechanical polishing. Additionally, the samples were cleaned using a plasma cleaner (FISCHIONE) of O_2^+Ar. To analyze the microstructure of the samples, a scanning electron microscope (SEM) focused ion beam (FIB) (FEI Helios NanoLab650) equipped with backscatter electron (BSE) and X-ray (EDX, Oxford X-MAX) detectors was used. Unless expressly indicated, the conditions for the micrographies were 10 kV and 0.8 nA, and 15 kV and 1.6 nA for the compositional analysis. Moreover, microstructural investigations during thermal cycling of the ε martensite were performed by in situ experiments, using a heating-cooling stage C1003 from Gatan, in a Schottky SEM (JEOL JSM-7000 F) equipped with BSE and X-ray (EDX, Oxford inca350) detectors. All microscopes are installed at the General Services of the UPV/EHU (SGIKER).

3. Experimental results

First, magnetic susceptibility measurements were carried out in order to determine the Neel temperature T_N of each alloy, in a SQUID MPMS-7 T from Quantum Design for FMS3 and FMS4 samples and using a magnetometer PPMS from Quantum Design for LMD sample. The importance behind determining the Neel temperature resides in the fact that, as commented, the magnetic transition from paramagnetic to anti-ferromagnetic state causes the stabilization of the γ phase, hence, the martensitic transformation is inhibited [28–30]. The obtained data, presented in Fig. 2, show that the alloy with the highest Neel temperature is the FMS3, in agreement with the composition of the alloy, because the Mn raises T_N whereas the Si content decreases T_N [3,27–30].

As commented before, Fe-Mn-Si alloys undergo a γ → ε martensitic transformation (MT), from the fcc γ austenite to the hcp ε martensite. The nucleation takes place through the motion of the

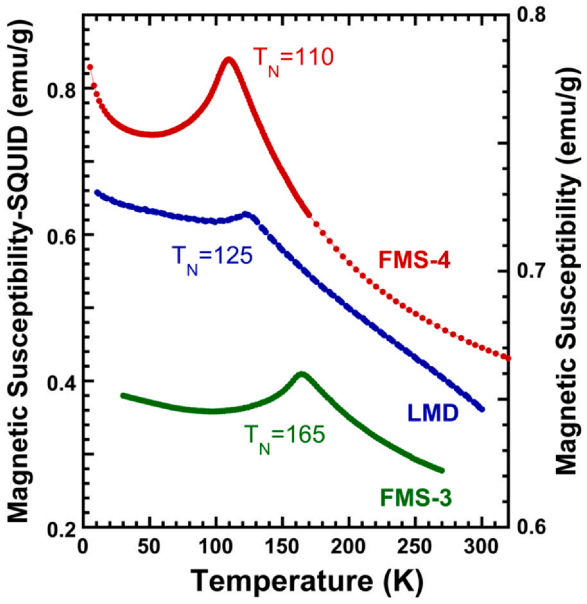

Fig. 2. Magnetic susceptibility measurements for determining the Neel temperature T_N. Left axis corresponds to samples FMS3 and FMS4, and the right axis to the LMD sample.

Shockley partial dislocations 1/6 < 112 > on a $\{111\}_{fcc}$ plane every two layers. This gliding of multiple Shockley partials cause a repositioning of atoms so that an hcp stacking fault is created, in between two Shockley partials, with a stacking ABAB inside the $\{111\}_{fcc}$ planes [34–36] given place to the embryo of ε martensite with the following orientation relationships: $(111)\gamma \parallel (0001)\varepsilon$ and $[11\text{–}2]\gamma \parallel [1\text{–}100]\varepsilon$, called Nishiyama relationships [4]. The growth of each single martensite plate is very fast through the motion of the Shockley partial, and the nucleation of multiple adjacent plates promotes the growth of thick plates and the progress of the transformation, see [20] for a recent review of these mechanisms. This slip-assisted mechanism as the origin for the martensitic transformation makes it non-thermoelastic [5,6], which means that although it exhibits a good shape memory and can be also stress-induced, does not exhibit a fully recoverable superelastic cycle. Independently of the non-thermoelastic character of the MT, it contributes to the internal friction and follows the behaviour described in the literature [33], contributing to the high damping associated with the MT [37].

In Fig. 3 the internal friction spectra and the dynamic modulus curves are shown for a complete transformation cycle of each one of the three alloys studied in this work: (a) FMS3, (b) FMS4 and (c) LMD. It can be easily identified the forward and reverse MT corresponding for each of the internal friction peaks and also associated with an abrupt change of the dynamic modulus (green). On cooling (blue), between Ms and Mf, the direct (or forward) transformation happens, in which the material transforms from γ austenite to ε martensite. On heating (red), between As and Af, the reverse transformation is observed from ε martensite to γ austenite. The temperature range between these phase transitions directly determinates the thermal hysteresis of the $\gamma \rightleftarrows \varepsilon$ transformation, being prominently high, as expected for a non-thermoelastic transformation [5,6], reaching values up to 170 K such as will be presented.

Moreover, the dynamic modulus variation associated with the forward and reverse transformation exhibits a hysteresis similar than the one of the IF peaks. It is also noticed that the modulus increases when the direct transformation occurs. This fact can be attributed to the progressive hardening of the microstructure because the ε martensite has a higher modulus than the γ austenite and

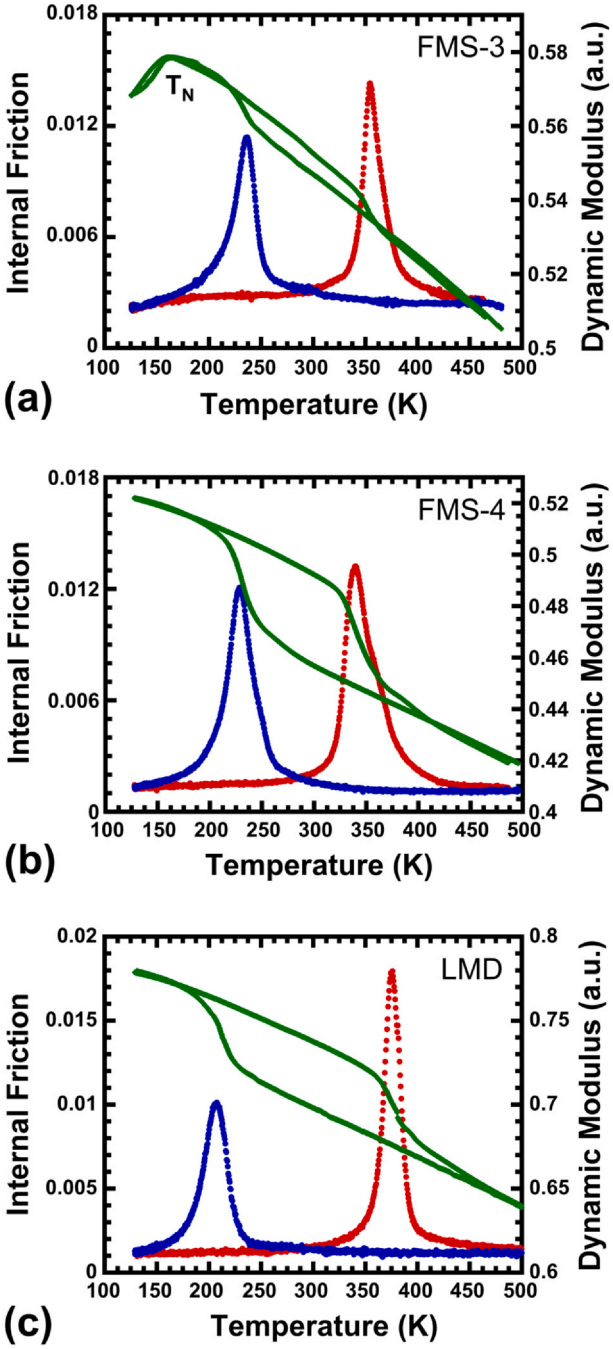

Fig. 3. Internal friction spectrum and dynamic modulus measurements versus temperature for (a) FMS3, (b) FMS4, (c) LMD samples. In blue, the forward martensitic transformation on cooling and, in red, the reverse martensitic transformation on heating.

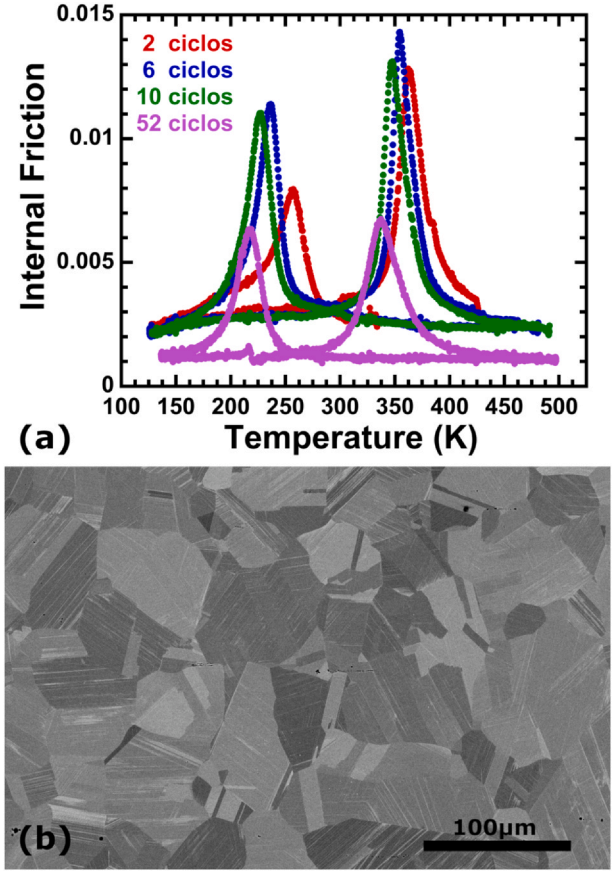

Fig. 4. (a) Evolution of the internal friction spectra on cycling for the FMS3 alloy. (b) Scanning electron microscopy BSE image for the same sample after 3 thermal cycles.

a rule of mixture can be applied in a first approach. So the hardening of the dynamic modulus will be proportional to the transformed fraction of ε martensite in a similar way than the IF peak. However, experimentally we have observed a slight deviation, when cooling the maximum of the derivative of modulus during forward MT takes place at about 4 K before than the IF peak. When heating, during the reverse MT the derivative of the modulus is also about 4 K above the IF peak. This phenomenon can be associated with the increasing internal stresses developed during the forward transformation, because the apparition of ε martensite produces a contraction of the lattice, involving the creation of dislocations, which are originated during the formation and growing of the martensite phase [38]. The developed elastic strains and stresses contribute to a supplementary increase of the dynamic modulus during the growing of martensite, being recovered during the reverse transformation. It should be also remarked that the drop of the dynamic modulus curve at about 160 K in FMS3 sample, in Fig. 3a, is due to the transition from paramagnetic to anti-ferromagnetic, as described in the literature [29], and in agreement with the measurements of the Neel Temperature T_N measured in Fig. 2, and consequently, such drop is not detected in FMS4 and LMD samples. All three alloys have $T_N < Mf$, therefore there is no interaction between the magnetic transition and the MT.

In what follows, the evolution of the MT on cycling will be presented for each one of the three samples, first the conventionally produced samples will be described, followed by the sample processed by additive manufacturing.

3.1. Samples from cast and rolling

The internal friction spectra, of the high Mn content sample with a Fe-20.2Mn-5.2Si-8.5Cr-5Ni composition, FMS3, evolve on cycling as can be seen in Fig. 4a. It is observed that the strength of the IF peaks increases rapidly during the first few thermal cycles, reaching a maximum for approximately the 6th cycle, from which it decreases smoothly. Since the internal friction measurements reflect the formation and movement of the martensite variants [26], it can be asserted that there is a maximum on the fraction of martensite plates transformed per cycle, which coincide with the maximum of the IF peaks [29]. Furthermore, as the cycling increases, the peaks shift as a whole towards low temperatures, meaning that the forward MT becomes delayed, exhibiting a hysteresis almost constant. For the 6th cycle (Fig. 4a), taking as reference the 50% of the

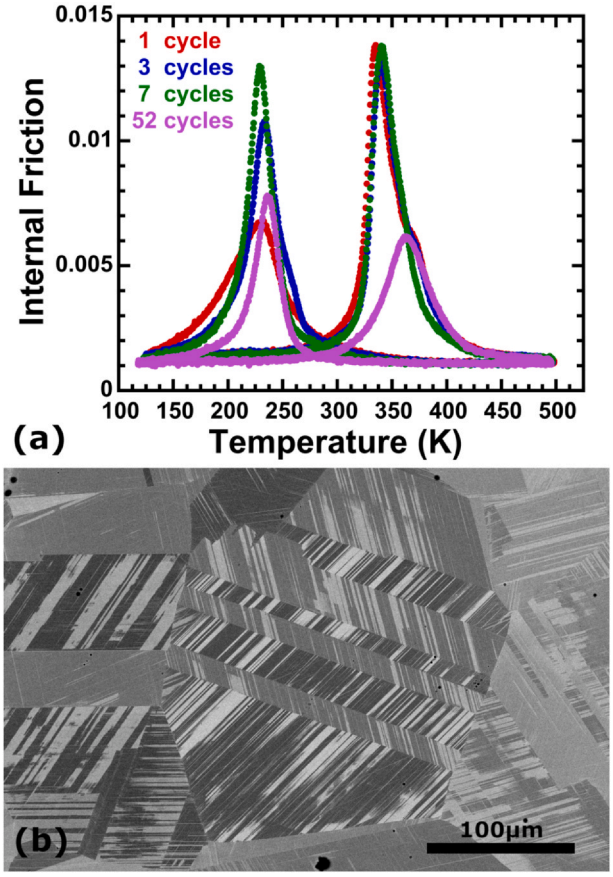

Fig. 5. (a) Evolution of the internal friction spectra on cycling for the FMS4 alloy. (b) Scanning electron microscopy BSE image for the same sample after 3 thermal cycles.

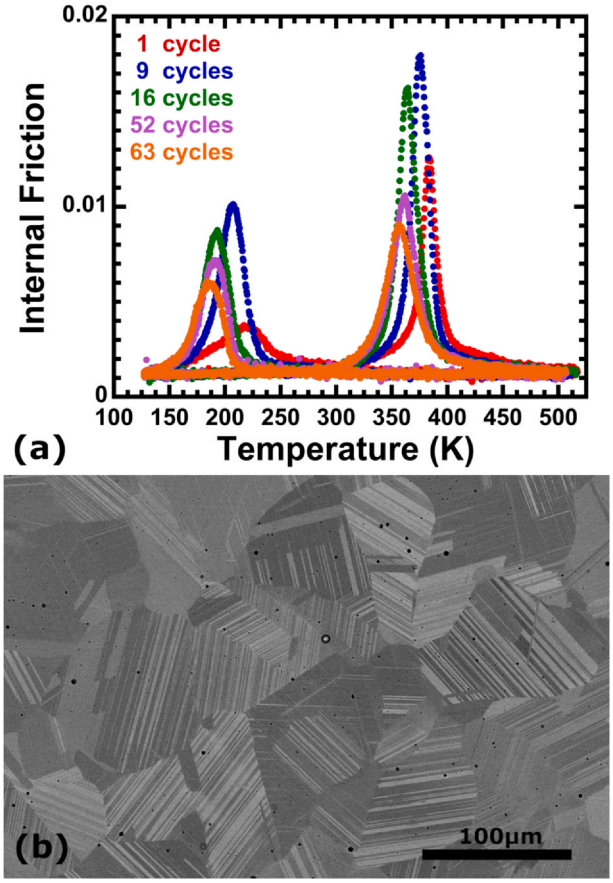

Fig. 6. (a) Evolution of the internal friction spectra on cycling for the LMD alloy produced by additive manufacturing. (b) Scanning electron microscopy BSE image for the same sample after 3 thermal cycles.

transformation, the forward transformation peak (Mp) occurs at 230 K and for the reverse transformation (Ap) at 357 K, hence, we obtain a hysteresis of almost 130 degrees. Nevertheless, it is important to mention that these peak temperatures (Mp and Ap) change with cycling; it exists a shifting towards lower temperatures as the number of cycles increases. For long term cycling, above 50 cycles, the IF peaks become smaller, what can be associated with an increase of the local stresses due to the slip-induced plasticity during the MT, which will deserve a further discussion.

To confirm the above description, a piece of the same sample was previously cut, polished and cycled outside, as described above, for its metallographic observation at the SEM. Fig. 4b presents a metallography after 3 cycles, in which the coexistence of γ austenite and ε martensite phases is revealed, and a big amount of ε martensite, shown as thin white plates, is already observed in agreement with the described evolution of the IF spectra.

The internal friction spectra of the low Mn content sample with a Fe-15.8Mn-6.1Si-9.2Cr-5Ni composition, FMS4, displayed in Fig. 5a, show a very similar behavior to the high Mn content alloy. The maximum strength of the internal friction appears in around the 7th cycle, which corresponds to a temperature Mp = 227 K for the direct transformation and Ap = 345 K for the reverse transformation, leaving a hysteresis of approximately 120 degrees. However, the change in the peak temperatures is not as pronounced as in FMS3 sample, moreover, in this case the shifting is towards higher temperatures of about 20 degrees in the first 50 cycles.

As in the previous case, the evolution of the microstructure on cycling was followed by SEM and in Fig. 5b the coexistence of γ and ε phases for the 3rd cycle can be also appreciated. The electron microscopy shows that the density of ε variants with the shape of thin white plates grew fast during the first cycles, which agrees with the IF peak area calculations.

3.2. Samples from additive manufacturing by LMD

The first and most remarkable fact from the LMD sample, with Fe-19.4Mn-5.9Si-9.2Cr-5.1Ni composition, is the existence of a noteworthy martensitic transformation behavior observed by IF, because this is the first time that the IF spectra were measured in an additive manufactured SMA of this family. Indeed, Fig. 6a shows the IF spectra evidencing the evolution of the MT on cycling. Following the examples previously mentioned, the internal friction peaks grow within the first few cycles, reaching a maximum transformed fraction in the 9th cycle. Then, during further cycling, the transformed fraction slowly decreases, evaluated through the integrated area of the IF peak, and a slight broadening of the peaks is observed, as the transformation requires a longer overcooling to complete. Furthermore, in comparison with the as-cast samples, the LMD sample presents a larger hysteresis. On the 9th cycle, displayed in Fig. 6a, the forward transformation occurs around Mp= 205 K and the reverse one around Ap= 375 K, achieving a hysteresis of almost 170 degrees based on the 50% of transformed fraction. On the other hand, it is also observed the shift on the direct and reverse transformation peaks towards lower temperatures, as in the case of the FMS3 sample, which seems to stabilize after approximately 80 cycles.

As in previous cases, Fig. 6b shows the microstructure after 3 thermal cycles, and this SEM metallography revealed that the fraction of martensite grows very fast at the beginning, and the ε plates become thicker within cycling. It should be remarked that this

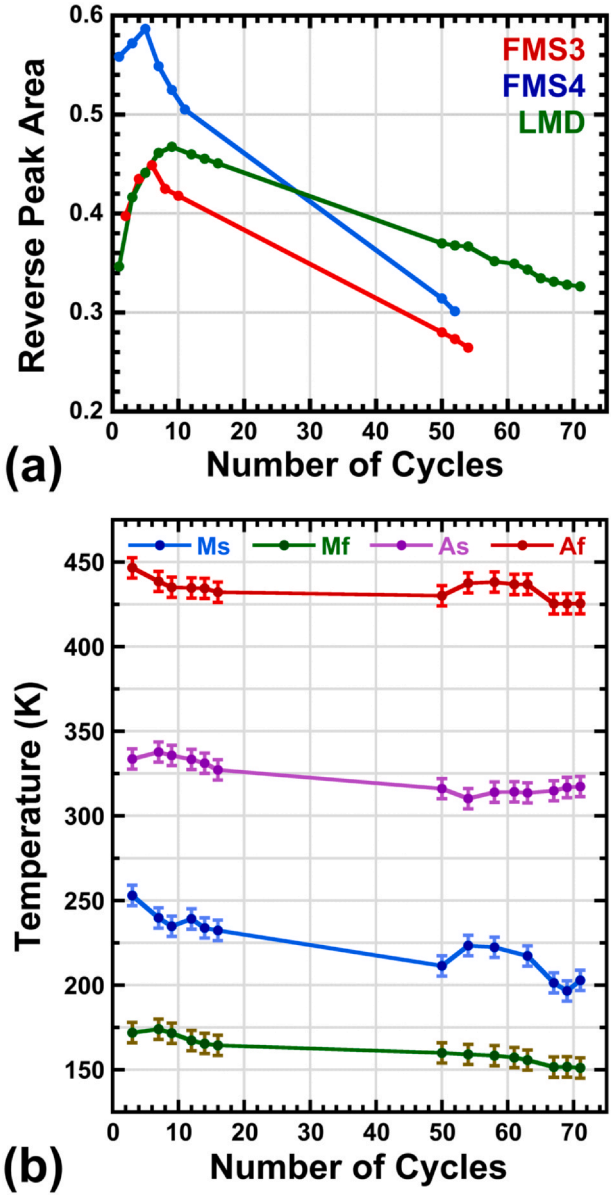

Fig. 7. (a) Calculated Internal friction peak area for the reverse transformation, as a function of the number of thermal cycles; FMS3 in red, FMS4 in blue and LMD in green. (b) Evolution of the martensitic transformation temperatures (Ms, Mf, As, Af) for the LMD sample.

additive manufactured alloy exhibits an extremely good and homogeneous transformation behavior as can be observed in Fig. 6.

4. Discussion

4.1. Evolution of the MT on cycling

All three samples exhibit a similar martensitic behavior, that is, the presence of a maximum in the internal friction peaks after a few number of thermal cycles, followed during further cycling by a global shift of the IF peaks and a decrease of the peak height and their integrated area. Nevertheless, there are some relevant points that must be discussed in order to do a comparative analysis of the behavior of the differently produced samples.

The integrated area of the IF peak is proportional to the martensite transformed fraction [29], and as commented previously this was calculated for the IF peak corresponding to the reverse MT. Then, in Fig. 7a, the integrated peak area for the reverse transformation is plotted for the three different alloys as a function of cycle number. It is observed that after about 6–9 cycles of fast growing, depending on the alloy, the ε fraction decreases. The behavior can be interpreted as follows. During the first cycles, when the direct transformation occurs, the martensite variants produce enough local stress, that accommodates plastically in the matrix and generates new dislocations in the γ structure, in the same (111) plane as the ε variants that produced them, remaining throughout the reverse transformation. As the number of thermal cycles rises, more nucleation points will happen and, consequently, the transformed fraction rapidly grows [27,29]. Moreover, the strength of the IF peaks is directly related to the transformation rate, undergoing an increase due to the greater amount of martensite in the same temperature interval. As the dislocation density increases in austenite, the stress field difficults the nucleation of the martensite and, as a non-thermoelastic alloy, enhances the existence of certain amount of local plastic deformation in the matrix and in the γ/ε boundaries [38,39]. This phenomenon hinders the growth of the martensite variants, leading to a stasis mechanism in which the volume of martensite does not achieve the 100% [40–42]. It also leads to a delay in the MT that explains the shift of the IF peaks in the subsequent cycles. Besides, the above statement also explains the decrease of the area inside the dynamic modulus on cycling. That is to say, the internal stresses prevent the motion of the dislocations in the γ matrix, hardening the microstructure and increasing the strength of the austenite [29,43]. This is in agreement with previous results on ternary Fe-Mn-Si alloys [44] where the transformed fraction decreases from the initial highly deformed state by further annealing. In our case the samples are recrystallized and the structure of dislocations is created during the first cycles, along which the fraction of ε martensite increases. Once a critical density of dislocations is created, associated with the increase of internal stresses, the transformed fraction of ε martensite decreases along cycling.

It is important to mention that the collected data of Fig. 7a offer a very outstanding result: the evolution of the martensite transformed fraction on cycling, decreases smoother for the LMD additive manufactured sample than for the conventionally produced samples, moreover it reflects a further stabilization in around cycle 80. Notwithstanding, the long-term cycling and its corresponding microstructural characterization still require additional research that is currently in progress.

On the other hand, when plotting the transformation temperatures, corresponding to the 5% and 95% of the transformed fraction, the temperatures undergo a shift towards lower temperatures. For the LMD sample, the results are presented in Fig. 7b, a slight variation of all transformation temperatures Ms, Mf, As and Af can be clearly noticed, but, although the IF peaks move practically as a whole, the shift is smoother for Mf, As and Af, in comparison with Ms that shifts up to 50 K for 72 cycles.

In the literature, there is still considerable controversy about the relation of the MT temperatures with thermal cycling in Fe-Mn-Si alloys. The great majority of studies, in agreement with our obtained data, show a decrease in the Ms, which can be explained as follows. As the density of nucleation points increases with cycling, the stress field difficults the formation and movement of the ε variants, and thus, a higher driving force is needed and the direct transformation temperature decreases [29]. Nonetheless, the reverse transformation temperatures are more incongruent. Some authors [39,42] show an increment in both As and Af for Fe-Mn-Si based alloys [39] and binary Fe-Mn alloys [42], whereas other authors [45] report a constant reverse transformation temperatures for Fe-27 wt%Mn-2.5 wt% Si. On the other hand, Sade et al. [46] reported that Ms descended only 10 K after 1000 thermal cycles between 598 K and Liquid Nitrogen, and As and Af increased due to the formation of transformation-induced lattice defects.

Finally, as previously mentioned, the hysteresis is significantly higher for the non-thermoelastic alloys [5,6], than for the more common Ni-Ti [7,8,47] or Cu-based [10,48] thermoelastic SMA [49]. The data obtained (from the 50% of transformed fraction) shows about 130 degrees for the high manganese content as-cast sample, 120 degrees for the low manganese content as-cast sample, and a remarkable almost constant 170-degree hysteresis for the LMD sample. The reason for which the LMD sample has a higher hysteresis than the as-cast samples is not yet fully understood, but seems to be associated with the particular microstructure developed during AM and must be further investigated.

4.2. Microstructural characterization of the MT

In parallel to the IF measurements, a microstructural characterization was performed by SEM on the samples undergoing the same thermal treatments and cycling than the ones used for IF. Then, in accordance with the internal friction measurements, during microstructural characterization it was observed that the fraction of transformed martensite grew fast within the first cycles, reaching a maximum for the 6–9 cycle and then the fraction decreased due to the too high internal stresses [27]. Nevertheless, the maximum of transformed fraction never reach the 100% of ε martensite, which underlines the existence of the reported stasis phenomenon [40].

Moreover, Fig. 8 shows a series of SEM images from an "in situ" cooling-heating experiment for the FMS4 sample, in which the sample was cooled to 110 K to thermally induce the forward MT and get the material in martensite, Fig. 8a, and then it was slowly heated up to 500 K to observe the reverse transformation Fig. 8b to f. It can be remarked that the transformation is fully completed, that is, all the ε plates revert to γ austenite, which also means that during the forward transformation there was no α' martensite formed by the intersection of ε plates [50], because the bcc martensite α' does not contribute to the shape memory effect and usually blocks the growing and motion of ε martensite [1,22].

The ε martensite plates nucleate in grain boundaries and grow towards the inner side of the austenite grain. If the grain is rather small, under approximately 30 µm [50], the ε plate grows till the boundary of opposite side, on the contrary, it could occur "the branching of the ε plate". When the direct MT takes place by the stacking of several stacking faults, the thicker the created ε plate, the larger it gets the elastic stresses at the tip of the growing ε plate. If the plate grows to a certain thickness, the elastic stress becomes large enough to make a new plate nucleate in a different plane $\{111\}_\gamma$ in order to reduce the elastic stresses at the tip of the preformed plate. Therefore, in the present work with an average grain size of around 100–150 µm after recrystallization, the metallographies show martensite plates following types III and IV as reported by Takaki et al. [50] for Fe-15%Mn. This phenomenon can be seen when comparing micrographies from the 3rd and 51st cycle for any of the alloys, where the plates in the second one are generally thicker. It is considered that the smaller the grain size is, the more stable the γ phase is and the less ε transformed fraction is achieved [40,51,52]. However, as the grain size grows, the possibility of getting α' also increases, but concerning this point, it seems that the prior γ grain size we obtained after recrystallization could said to be satisfactory. This correlation could also support the fact that the sample FMS3, with a smaller average grain size, presented less transformed fraction as shown in Figs. 3a and 7a. Nevertheless, the optimal grain size also depends on the elaborating process [53], and the effect of the multiple variables participating during additive manufacturing [23–25] must be further analyzed.

Another aspect that must be emphasized is the reproducibility of the martensitic transformation. In Fig. 9, in the SEM images taken for the first (a-b) and second (c-d) thermal transformation on cooling, it can be appreciated that the ε plates were originated in the same nucleation points where the plates formed in the previous forward transformation, creating two similar patterns. The distinguishable difference resides in the length and thickness of the plates, which grow fast along the first cycles, as discussed previously [50]. Thus, it can be concluded that the partial dislocations move reversibly in the forward and reverse MT, so that there is no interaction between crossed ε martensite plates and no α' is formed, consequently the structure of the austenite does not change by thermal cycling and reproducibility of ε happens. This result is in accordance with previous works of Shiming et al. [54], who reported a small but

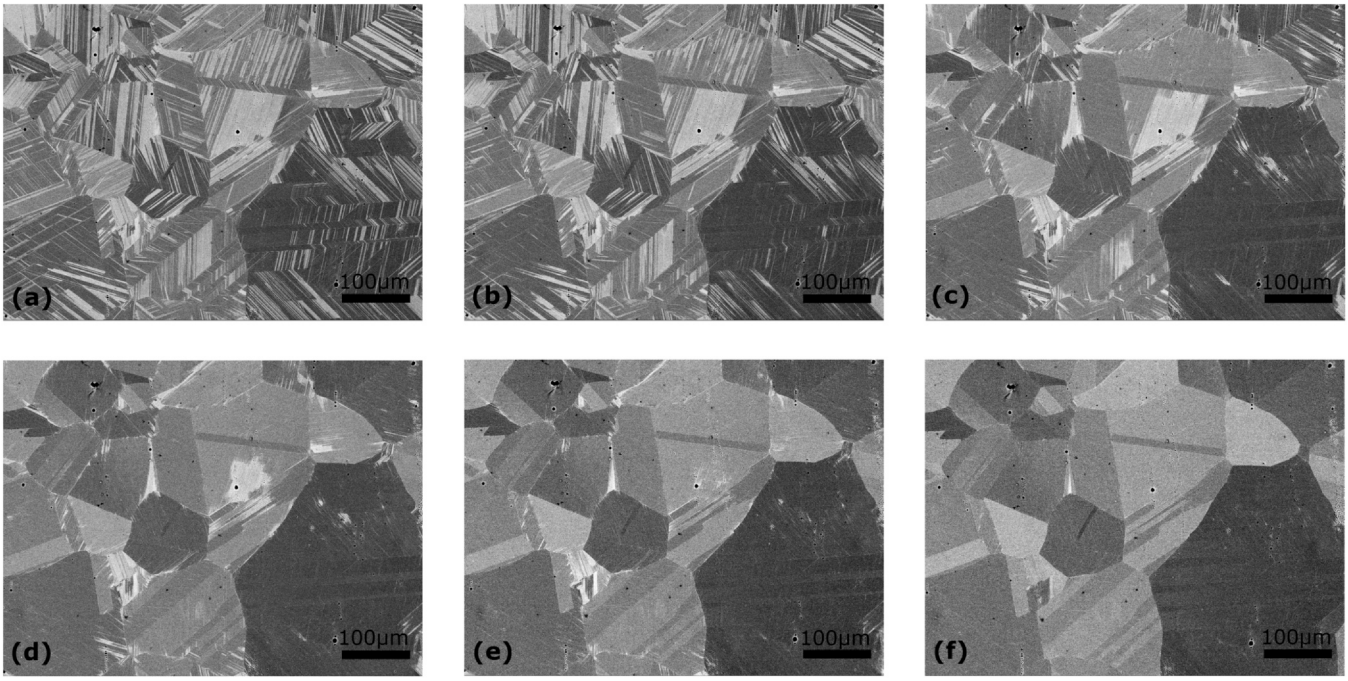

Fig. 8. Scanning electron microscopy BSE images taken during an "in situ" experiment for the FMS4 sample: (a) Martensite formed after cooling down to 110 K. (b) to (f) Images taken during slow heating up to 500 K, showing the evolution of the reverse martensitic transformation.

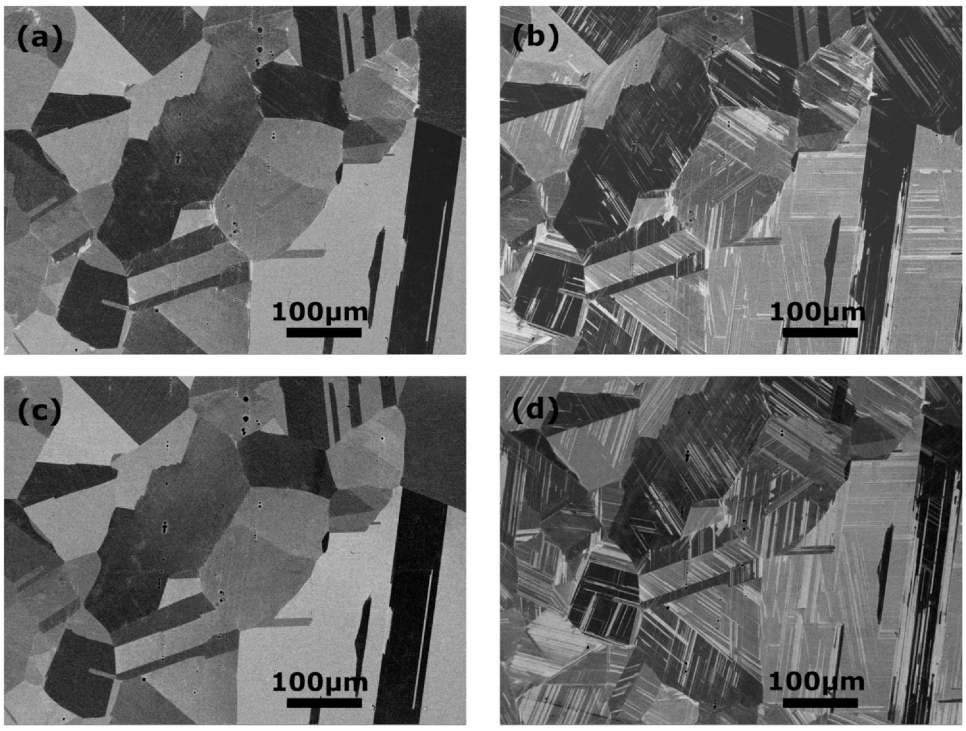

Fig. 9. Scanning electron microscopy BSE images of the FMS4 sample for the first two thermal cycles: (a) First cycle, austenite at 500 K. (b) First cycle, martensite after cooling down to 110 K. (c) Second cycle, austenite at 500 K. (d) Second cycle, martensite after cooling down to 110 K.

perceptible two-way shape memory effect in a Fe-29.4Mn-6.2Si alloy, due to the reversible movement of partial dislocations. Moreover, good microstructure memory and reproducibility was also reported by Tsuzaki et al. [43] when cycling a Fe-24Mn-6Si alloy up to 573 K (above Af), arguing that this memory is closely related to the degree of recovery of austenite during reverse heating.

5. Conclusions

The non-thermoelastic martensitic transformation of Fe-Mn-Si-Cr-Ni with different compositions and production methods were characterized by mechanical spectroscopy, evidencing a reproducible MT, followed through the internal friction peaks, exhibiting the high hysteresis associated with this kind of alloys. Remarkably, the martensitic behavior for the samples produced by the additive manufacturing technique of LMD (Laser Metal Deposition) was shown to be more satisfactory, in what concerns the transformed fraction of reversible ε martensite, calculated from the peak areas. On the other hand, a microstructural analysis was carried out by electron microscopy and "in-situ" experiments where the complete thermal cycles were observed. The results showed that a complete recovery of the ε martensite is achieved during reverse transformation. Furthermore, a good reproducibility and crystallographic reversibility during thermal cycling was observed, being attributed to the reversible movement of partial dislocations, that is, ε plates always originate in the same nucleation points and lengthen and thicken as the number of cycles increases.

Two main ideas can be also summarized. The mechanical spectroscopy, through the internal friction and dynamic modulus measurements, is a powerful tool to study the martensitic transformation in non-thermoelastic shape memory alloys. The additive manufacturing technologies reveal as a good production methodology to obtain functional specimens and devices of Fe-Mn-Si-Cr-Ni shape memory alloys, opening new avenues for the development of unforeseen applications of this family of shape memory steels.

Declaration of Competing Interest

The authors declare that they have no known competing financial interests or personal relationships that could have appeared to influence the work reported in this paper.

Acknowledgements

This work was supported by the ELKARTEK-CEMAP (KK-2020/00047) project from the Industry Department of the Basque Government, and the GIU-17/071 from the University of the Basque Country, UPV/EHU. This work made use of the SGIKER facilities at the UPV/EHU.

References

[1] A. Sato, E. Chishima, K. Soma, T. Mori, Shape memory effect in γ-ε transformation in Fe-30Mn-1Si alloy single crystals, Acta Metall. 30 (1982) 1177–1183.
[2] A. Sato, E. Chishima, Y. Yamaji, T. Mori, Orientation and composition dependencies of shape memory effect in Fe-Mn-Si alloys, Acta Metall. 32 (1984) 539–547.
[3] M. Murakami, H. Suzuki, Y. Nakamura, Effect of Si on the shape memory effect of polycristalline Fe-Mn-Si alloys, J. Trans. Iron Steel Inst. Jpn. 27 (3) (1986) 87–92.
[4] Z. Nishiyama, Martensitic Transformation, Academic Press, New York, USA, 1978.
[5] Q. Gu, J. Van Humbeeck, J. Delaey, A review on the martensitic transformation and shape memory effect in Fe-Mn-Si alloys, J. Phys. IV 3 (1994) 135–144.
[6] T. Maki, Ferrous Shape Memory Alloys, in: K. Otsuka, C.M. Wayman (Eds.), Shape Memory Materials, Chapter 5 Cambridge University Press, Cambridge, UK, 1998, pp. 117–132.
[7] K. Otsuka, X. Ren, Physical metallurgy of Ti-Ni-based shape memory alloys, Prog. Mater. Sci. 50 (2005) 511–678.
[8] K. Yamauchi, I. Ohkata, K. Tschiya, S. Miyazaki (Eds.), Shape memory and superelastic alloys, Woodhead Publishing, Oxford, UK, 2011.
[9] K. Otsuka, C.M. Wayman (Eds.), Shape Memory Materials, Cambridge University Press, Cambridge, UK, 1998.
[10] I. López-Ferreño, J.F. Gómez-Cortés, T. Breczewski, I. Ruiz-Larrea, M.L. Nó, J.M. San, Juan, High-temperature shape memory alloys based on the Cu-Al-Ni system: design and thermomechanical characterization, J. Mater. Res. Technol. 9 (2020) 9972–9984.
[11] T. Maruyama, T. Kurita, S. Kozaki, K. Andou, S. Farjami, H. Kubo, Innovation in producing crane rail fishplate using Fe-Mn-Si-Cr based shape memory alloy, Matter Sci. Tech. 24 (2008) 908–912.

[12] T. Maruyama, H. Kubo, Ferrous shape memory alloys: properties, processing and applications. In Ref. [8], chapter 12, pp 141–159, 2011.
[13] A.V. Druker, A. Perotti, I. Esquivel, J. Malarria, A manufacturing process for shaft and pipe couplings of Fe-Mn-Si-Ni-Cr shape memory alloys, Matter Des. 56 (2014) 878–888.
[14] A. Cladera, B. Weber, C. Leinenbach, C. Czaderski, M. Shahverdi, M. Motavalli, Iron-based shape memory alloys for civil engineering structures: an overview, Constr. Build. Mater. 63 (2014) 218–293.
[15] Y. Watanabe, E. Miyazaki, H. Okada, Enhanced mechanical properties of Fe-Mn-Si-Cr shape memory fiber/plaster smart composite, Mater. Trans. 43 (2002) 974–983.
[16] Z.X. Zhang, J. Zhang, H. Wu, Y. Ji, D.D. Kumar, Iron-based shape memory alloys in construction: research applications and opportunities, Materials 15 (2022) 1723.
[17] N. Igata, K. Nishiyama, K. Ota, Y. Yin, W. Wuttig, I.S. Golovin, J.V. Humbeeck, J. San Juan, Panel discussion on the application of high damping materials, J. Alloy. Comp. 355 (2003) 230–240.
[18] I. Nikulin, N. Nagashima, F. Yoshinaka, T. Sawaguchi, Superior fatigue life of Fe-15Mn-10Cr-8Ni-4Si seismic damping alloy subjected to extremey high strain amplitudes, Mater. Lett. 230 (2018) 257–260.
[19] T. Sawaguchi, I. Nikulin, K. Ogawa, S. Takamori, F. Yoshinaka, Y. Chiba, H. Otsuka, Y. Inoue, A. Kushibe, Low-cycle fatigue life and plasticity mechanisms of a Fe-15Mn-10Cr-8Ni-4Si seismic damping alloy under cyclic loading at various temperatures, Acta Mater. 220 (2021) 117267.
[20] P. Chowdhury, D. Canadinc, H. Sehitoglu, On deformation behavior on Fe-Mn based structural Alloys, Mater. Sci. Eng. R. 122 (2017) 1–28.
[21] Y.H. Wen, H.B. Peng, D. Raabe, I. Gutierrez-Urrutia, J. Chen, Y.Y. Du, Large recovery strain in Fe-Mn-Si-based shape memory steel obtained by engineering annealing twin boundaries, Nat. Comm. 5 (2014) 4964.
[22] H. Peng, J. Chen, Y. Wang, Y. Wen, Key factors achieving large recovery strain in polycrystalline Fe-Mn-Si-based shape memory alloys: a review, Adv. Eng. Mater. 20 (2018) 1700741.
[23] D. Herzog, V. Seyda, E. Wycisk, C. Emmelmann, Additive manufacturing of metals, Acta Mater. 117 (2016) 371–392.
[24] J.O. Milewski, Additive Manufacturing of Metals, Springer Int. Publishing, 2017.
[25] M. Elahinia, N.S. Moghaddam, M.T. Andani, A. Amerinatanzi, B.A. Bimber, R.F. Hamilton, Fabrication on NiTi through additive manufacturing: a review, Prog. Mater. Sci. 83 (2016) 630–663.
[26] J. San, Juan, Mechanical spectroscopy, Mater. Sci. Forum 366–368 (2001) 32–73.
[27] R.B. Peréz-Saéz, Estudio Mediante Fricción Interna de la Transformación Martensítica. Aleaciones con Memoria de Forma de Cu-Al-Ni Elaboradas por Pulvimetalurgia y de Fe-Mn-Si-Cr-Ni (PhD Thesis), University of the Basque Country, UPV/EHU,, Bilbao, Spain, 1998.
[28] M. Murakami, H. Otsuka, G. Suzuki, S. Matsuda, Complete shape memory effect in polycrystalline Fe-Mn-Si alloys, Proc. ICOMAT-86, Nara, Japan, August 1986. The Japan Institute of Metals (1987) 985–990.
[29] R.B. Pérez-Sáez, M.L. Nó, J. San, Juan, Internal friction in Fe-Mn-Cr-Si-Ni shape memory alloys, J. Alloy. Comp. 211/212 (1994) 212–215.
[30] X.J. Jin, T.Y. Hsu, X. Zuyao, Thermodynamic consideration of antiferromagnetic transition on fcc (γ)→hcp (ε) martensitic transformation in Fe-Mn-Si shape memory alloys, Mater. Chem. Phys. 61 (1999) 135–138.
[31] L. Federzoni, Etude d'un acier inoxidable à mémoire de forme (PhD Thesis), INSA Lyon, France, 1993.
[32] I. Gutierrez-Urrutia, M.L. Nó, E. Carreño-Morelli, B. Guisolan, R. Schaller, J. San Juan, High performance very low frequency forced pendulum, Mater. Sci. Eng. A 370 (2004) 435–439.
[33] J. San Juan, R.B. Pérez-Sáez, Transitory effects, Mater. Sci. Forum 366- 368 (2001) 416–436.
[34] A. Bogers, W. Burgers, Partial dislocations on the {110} planes in the BCC lattice and the transition of the FCC into the BCC lattice, Acta Met. 12 (1964) 255–261.
[35] G. Olson, M. Cohen, A general mechanism of martensitic nucleation: Part I. General concepts and the FCC-HCP transformatio, Metall. Trans. A 7 (1976) 1897–1904.
[36] G. Olson, M. Cohen, A general mechanism of martensitic nucleation: Part II. FCC-BCC and other martensitic transformations, Metall. Trans. A 7 (1976) 1905–1914.
[37] J. San Juan, M.L. Nó, Damping behavior during martensitic transformation in shape memory alloys, J. Alloy. Comp. 355 (2003) 65–71.
[38] R.B. Pérez-Sáez, M.L. Nó, J. San Juan, Influence of thermal cycling in a Fe-Mn-Si-Cr-Ni shape memory alloy, J. De. Phys. III 5 (1995) 443–448.
[39] J. Hong, S. Choi, Y. Lee, Stasis mechanism of γ→ε martensitic transformation in Fe-17Mn alloy, Acta Mater. 210 (2021) 116846.
[40] K. Tsuzaki, M. Ikegami, Y. Tomota, T. Maki, Effect of transformation cycling on the ε martensitic transformation in Fe-Mn alloys, ISIJ Int. 30 (1990) 666–673.
[41] N. Nakada, Y. Ishibashi, T. Tsuchiyama, S. Takaki, Self-stabilization of untransformed austenite by hydrostatic pressure via martensitic transformation, Acta Mater. 110 (2016) 95–102.
[42] A.M. Balagurov, I.A. Bobrikov, J. Pons, J. Cifre, L.Y. Sun, I.S. Golovin, Structure of the Fe-Mn-Si alloys submitted to γ ↔ ε thermocycling, Mater. Charact. 141 (2018) 223–228.
[43] K. Tsuzaki, M. Ikegami, Y. Tomota, Y. Kurokawa, W. Nakagawara, T. Maki, Effect of thermal cycling on the martensitic transformation in an Fe-24Mn-6Si shape memory alloy, Mater. Trans. JIM 33 (1992) 263–270.
[44] L. Sun, W.C. Cheng, A.M. Balagurov, I.A. Bobrikov, J. Cifre, I.B. Chudakov, S.U. Jen, V. Cheverikin V., M.Y. Zadorozhnyy, I.S. Golovin, Effect of thermal cycling on microstructure and damping capacity of Fe-26Mn-4Si alloy, Mater. Charact. 159 (2020) 110001.
[45] M.S. Andrade, R.M. Osthues, G.J. Arruda, The influence of thermal cycling on the transition temperatures of a Fe-Mn-Si shape memory alloy, Mater. Sci. Eng. A 273–275 (1999) 512–516.
[46] M. Sade, K. Halter, E. Hornbogen, The effect of thermal cycling on the transformation behaviour of Fe-Mn-Si shape memory alloys, Z. Metallkd. 79 (1988) 487–491.
[47] J. Frenzel, E.P. George, A. Dlouhy, C. Somsen, M.F.X. Wagner, G. Eggeler, Influence of Ni on martensitic phase transformations in NiTi shape memory alloys, Acta Mater. 58 (2010) 3444–3458.
[48] R. Kainuma, S. Takahashi, K. Ishida, Thermoelastic martensite and shape memory effect in ductile Cu-Al-Mn alloys, Met. Mater. Transit. A 27 (1996) 2187–2195.
[49] J. Van Humbeeck, R. Stalmans, Characteristics of shape memory alloys, in Ref. [9], Chap. 7, 149–183, 1998.
[50] S. Takaki, H. Nakatsu, Y. Tokunaga, Effects of Austenite Grain Size on ε Martensitic Transformation in Fe-15mass%Mn Alloy, Mater. Trans. JIM 34 (1993) 489–495.
[51] P. La Roca, A. Baruj, M. Sade, Shape-memory effect and pseudoelasticity in Fe–Mn-Based Alloys, Shape Mem. Superelasticity 3 (2017) 37–48.
[52] A.V. Druker, P. Vermaut, J. Malarria, The Shape recovery conditions for the Fe-Mn-Si alloys: an interplay between martensitic transformation and plasticity, Mater. Charact. 139 (2018) 319–327.
[53] A.V. Druker, A. Baruj, L. Isola, V. Fuster, J. Malarría, R. Bolmaro, Gaining flexibility in the design of microstructure, texture and shape memory properties of an Fe-Mn-Si-Cr-Ni alloy processed by ECAE and annealing, Mater. Des. 107 (2016) 153–162.
[54] T. Shiming, L. Jinhai, Y. Shiwei, Two-way shape memory effect of an Fe-Mn-Si alloy, Scr. Metall. Mater. 25 (1991) 1119–1121.